Supplementary Information (SI) for New Journal of Chemistry.

Supplementary Materials for

Low carbon to metal ratio and nucleation of hexagonal moiré superlattices in onion-like graphitic-domains within the walls of carbon nanotubes by pyrolysis of ferrocene in viscous boundary layers

Filippo S. Boi[a]*, Lin Zhang[a], Xilong Guo[a], Jian Guo[a], Hansong Wu[a] and Shanling Wang[b]

a. College of Physics, Sichuan University, Chengdu, China.

b. Analytical and Testing Centre, Sichuan University, Chengdu, China.

*Email corresponding author: f.boi@scu.edu.cn,

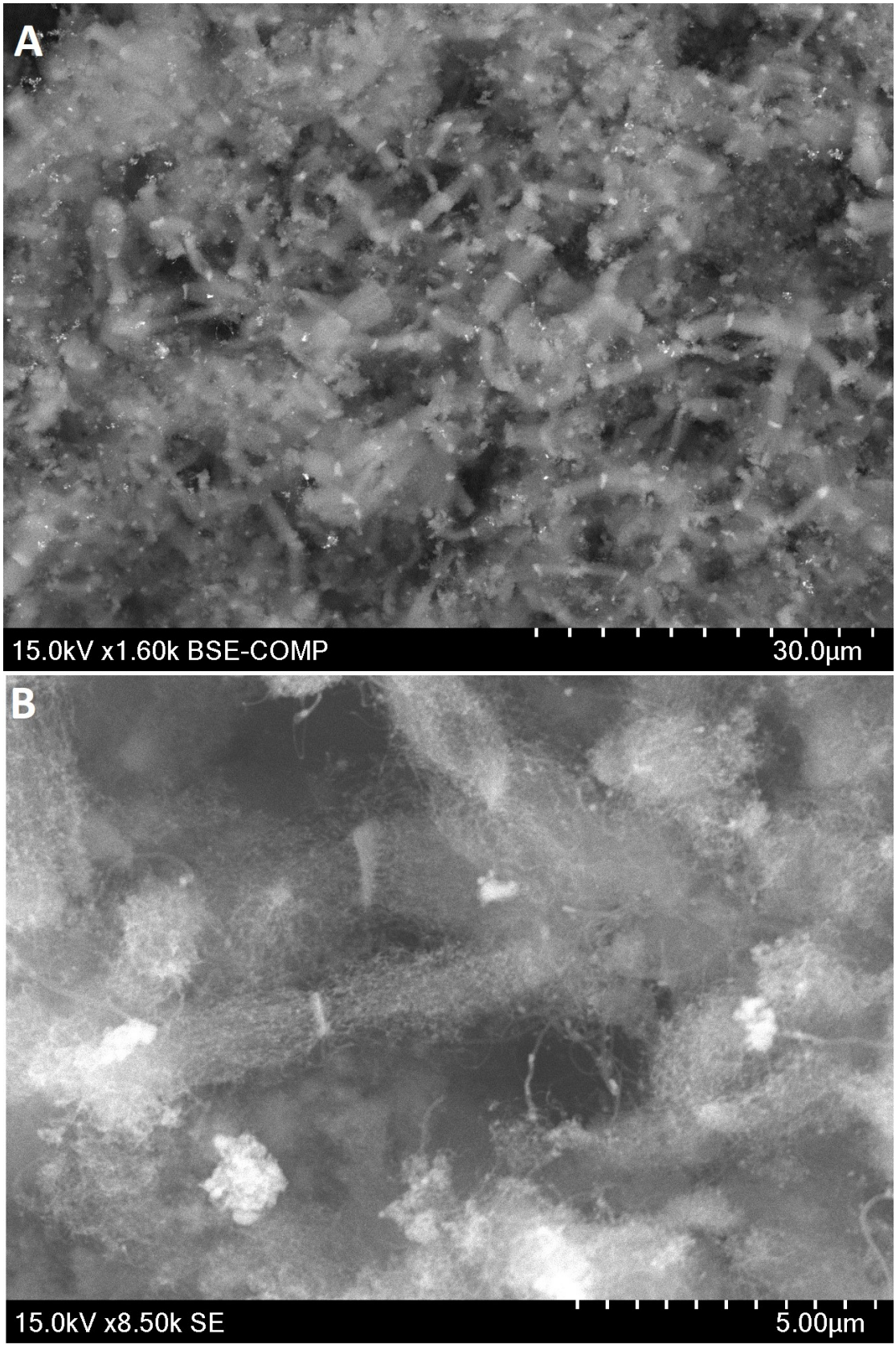

Figure S1: SEM micrographs acquired with backscattered (A) and secondary (B) electrons revealing the nucleation of large amounts of radial CNT structures.

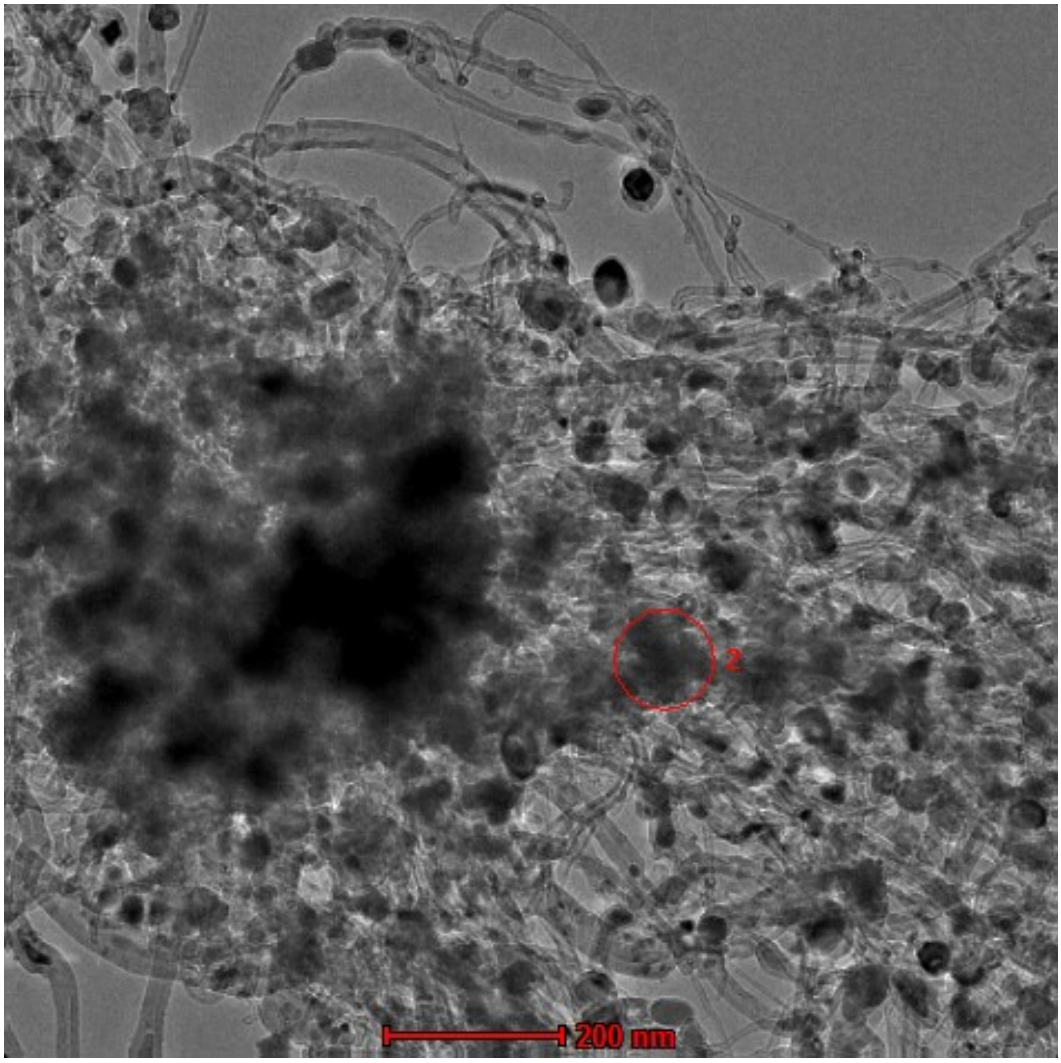

Figure S2: HRTEM of a radial structure obtained by pyrolysis of ferrocene in a viscous boundary layer. The red circle identifies the region from where the EDX spectrum was taken.

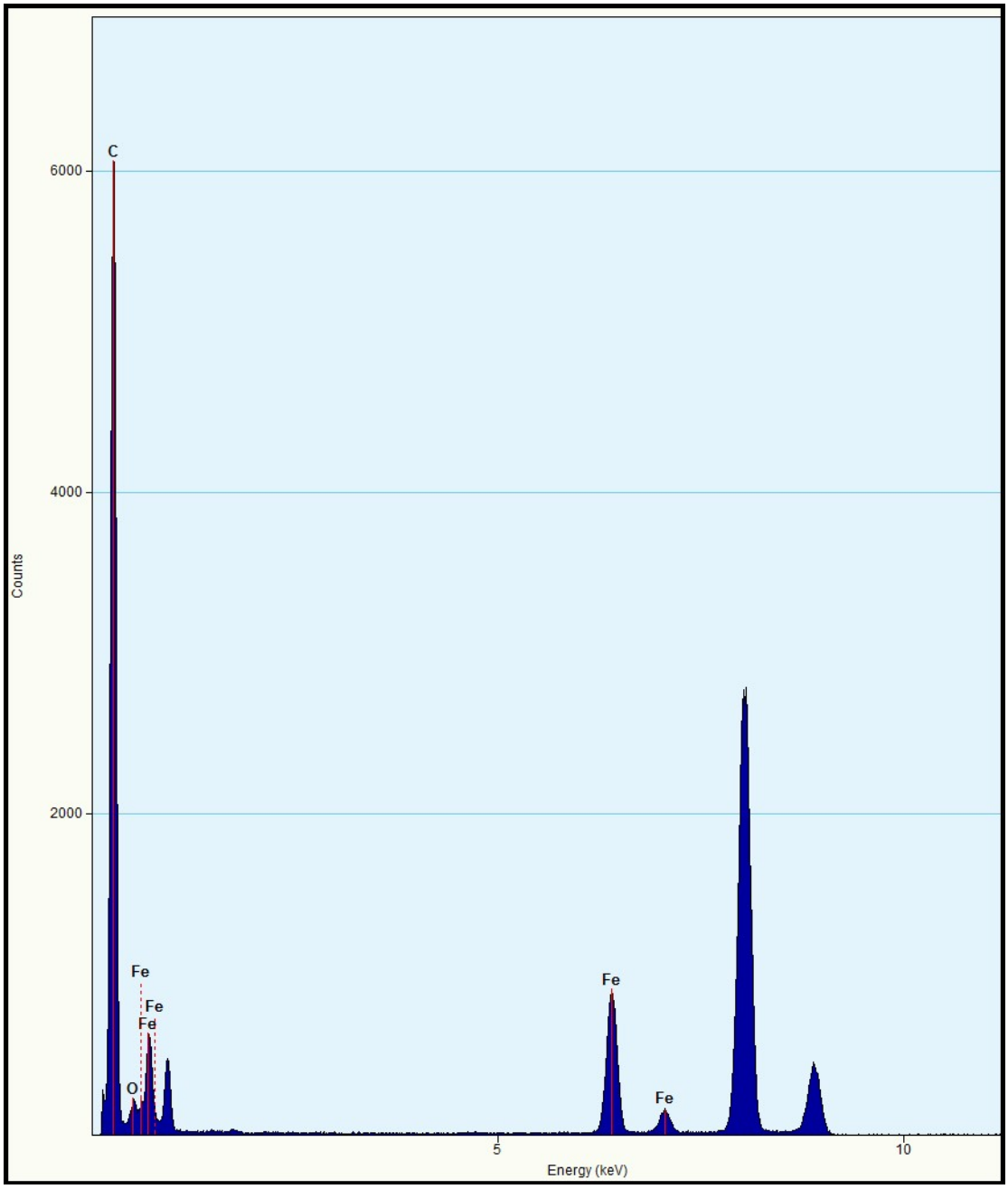

Figure S3: EDX spectrum acquisitions from the radial structure selected in Fig.S2 (red-circle).

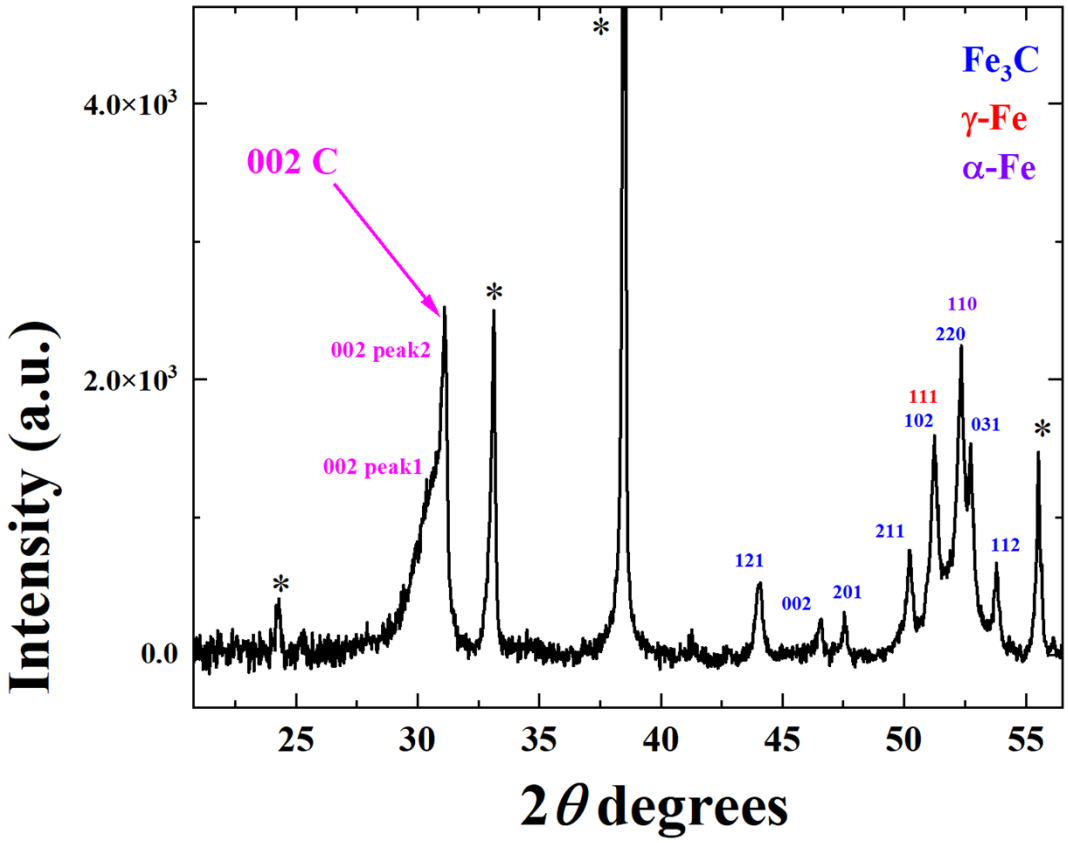

Figure S4: XRD analyses of as grown radial structures, revealing the presence of a splitting in the diffraction peak originating from graphitic carbon. The observed structural transition is attributable to the coexistence of onion-like and nanotube graphitization in the sample [36]. The stars identify signals arising from the Si-substrate.

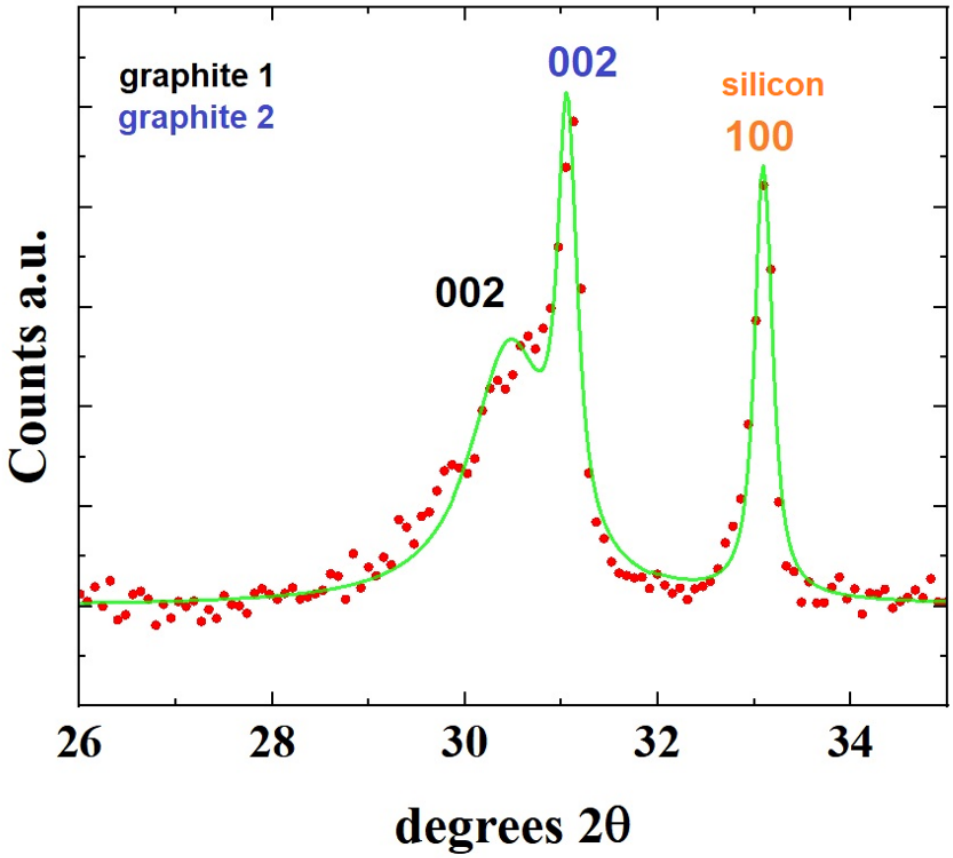

Figure S5: XRD diffractogram (red) and Rietveld refinement (green line) revealing an asymmetric (0 0 2) diffraction peak, arising from the multilayered graphitic lattices of the CNT/CNO layers in the sample. These observations are also indicative of a distorted c-axis parameter, which was found to vary from 6.69Å (graphite-1 peak) to 6.82Å (graphite-2 peak), with the relative abundance being 28.12% (graphite phase-1) and 71.88% (graphite phase-2), when excluding the contribution from the metal catalyst.

Table 1: List exhibiting the lattice parameters and relative abundance of the encapsulated nanocrystal phases identified in the radial CNT/CNO sample. The relative abundance is calculated by excluding the graphitic carbon.

Table 1	Lattice parameter						Relative abundance
	a	b	c	α	β	γ	
Fe_3C	5.10Å	6.75Å	4.53Å	90°	90°	90°	52.20%
γ-Fe	3.59Å	3.59Å	3.59Å	90°	90°	90°	27.87%
α-Fe	2.87Å	2.87Å	2.87Å	90°	90°	90°	19.93%

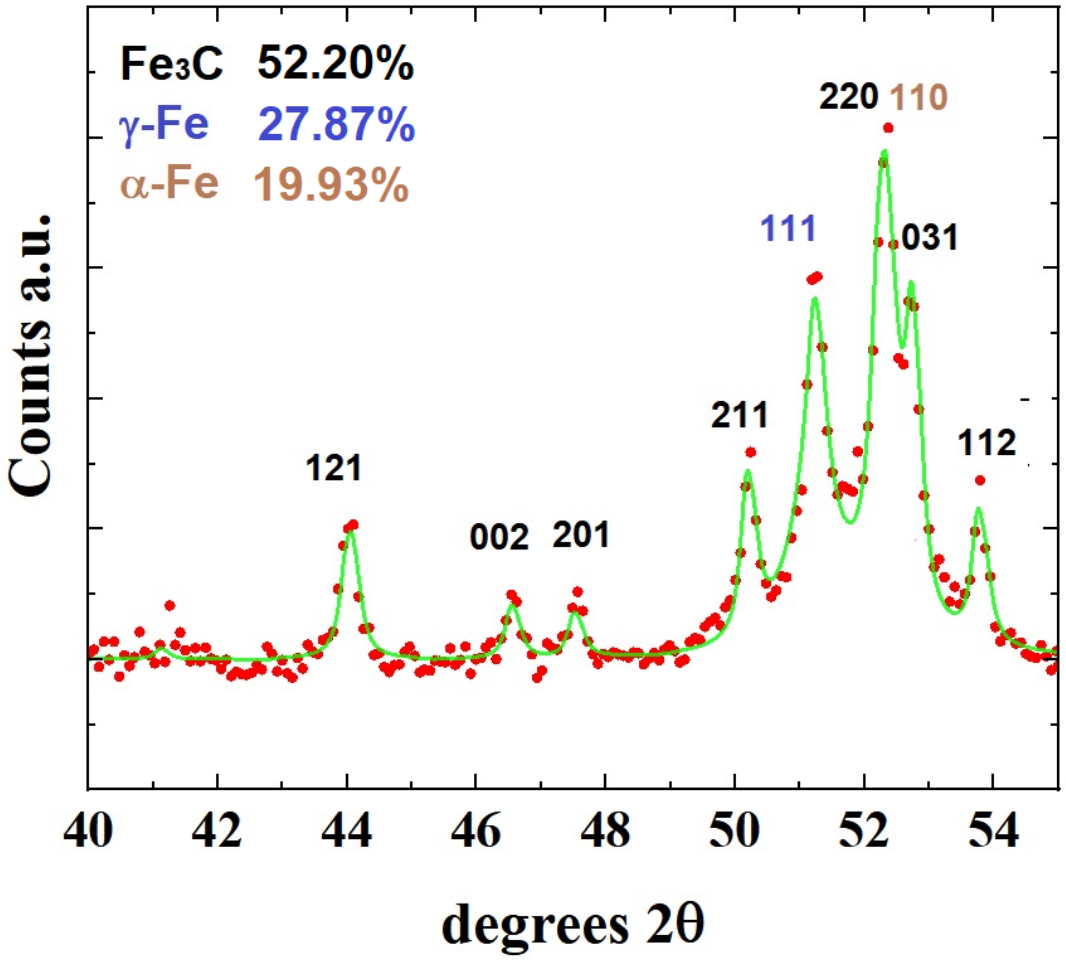

Figure S6: XRD and Rietveld refinement analyses revealing the structural characteristics of the nanocrystals encapsulated within the CNTs and CNOs.

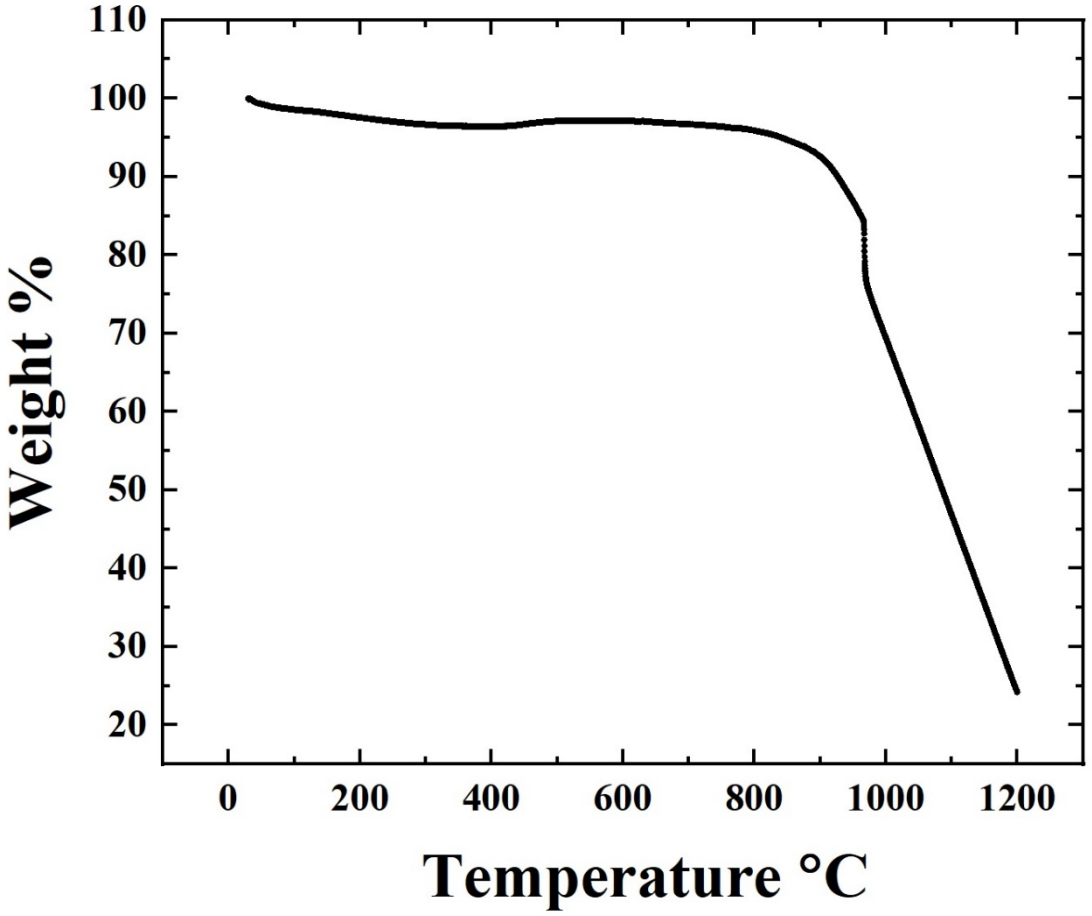

Figure S7: TGA analyses (under N_2 flow) revealing a rapid decomposition of the CNT/CNOs structures above 900 °C.

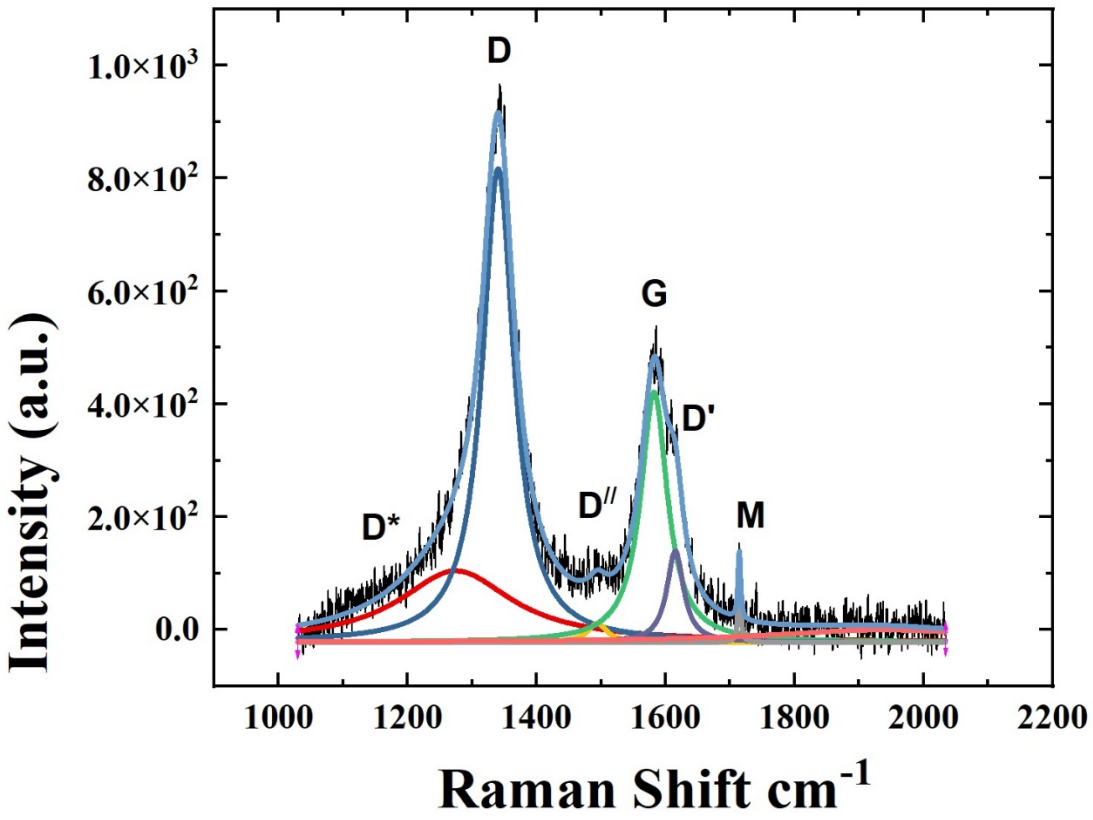

Figure S8: Raman spectroscopy analyses in the Raman shift range from 1000 to 2025 cm^{-1}, revealing the presence of an intense D band attributable to disordered induced scattering produced by imperfections/defects or loss of hexagonal symmetry within the stacking-fault rich graphitic carbon layers of the radial CNOs/CNTs structures, in coexistence with the G band (active $2E_{2g}$ mode indicative of the symmetry of the hexagonal lattice) and D' (indicative of contributions arising from specific types of structural defects in the graphitic lattice of the CNOs and CNTs) signals. An ID/ID' ratio ~ 5.9 could be extracted, which is indicative of boundary defects [Ref.S1]. The D* and D$^{//}$ bands identify contributions arising from weakly oxidized interfaces.

[Ref.S1] Axel Eckmann, Alexandre Felten, Artem Mishchenko, Liam Britnell, Ralph Krupke, Kostya S. Novoselov and Cinzia Casiraghi. Probing the Nature of Defects in Graphene by Raman Spectroscopy. Nano Lett. 2012, 12, 8, 3925–3930

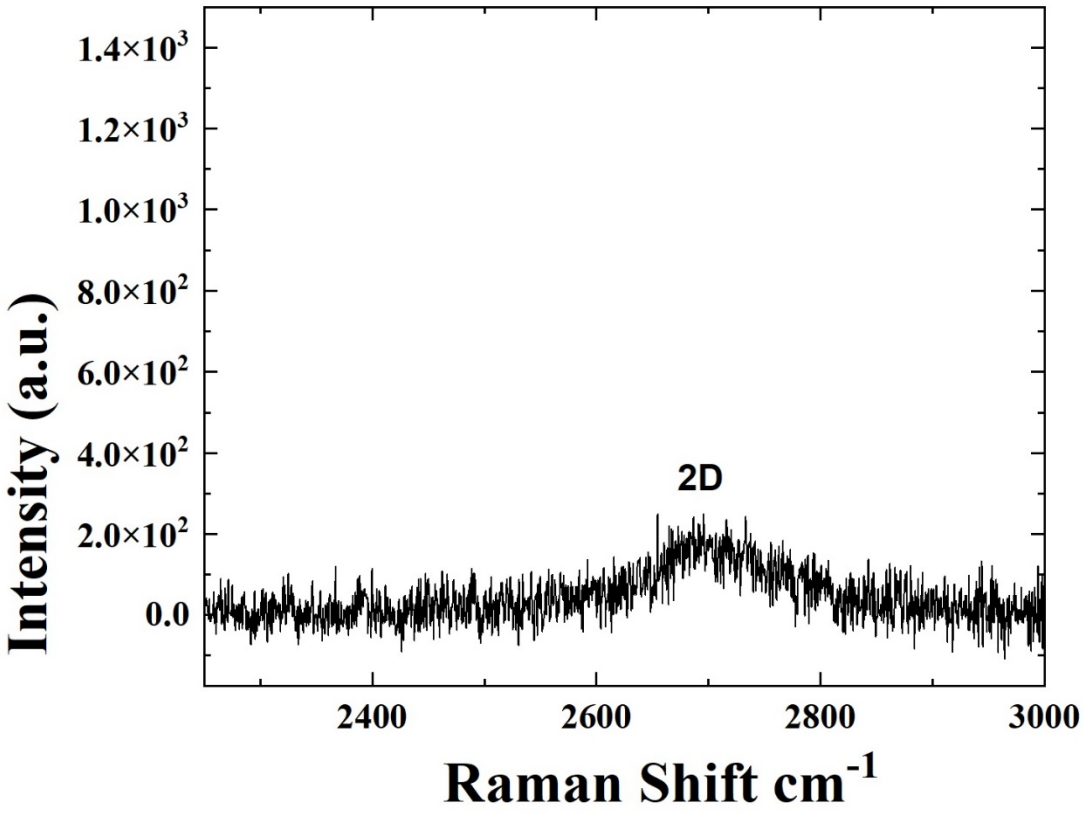

Figure S9: Raman spectroscopy analyses in the Raman shift range from 2200 to 3000 cm^{-1}, revealing the presence of a broad 2D band, deriving from contributions of the coexisting multilayered CNO and CNT morphologies.